Zero-Plane Displacement Height in a Highly Built-Up Area of Tokyo

Shinya Tanaka[1], Hirofumi Sugawara[1], Ken-ichi Narita[2], Hitoshi Yokoyama[3], Ikusei Misaka[4], and Dai Matsushima[5]
[1]*National Defense Academy of Japan, Yokosuka, Japan*
[2]*Nippon Institute of Technology, Saitama, Japan*
[3]*Tokyo Metropolitan Resesarch Institute for Environmental Protection, Tokyo, Japan*
[4]*Takenaka Corporation, Chiba, Japan*
[5]*Chiba Institute of Technology, Chiba, Japan*

Abstract

The zero-plane displacement height *d* was evaluated in downtown Tokyo by the two independent methods of temperature variance and scintillometer heat flux. Regardless of the method, *d* exceeds the area-weighted average building height. This may be because *d*, which represents the point of effect for wind drag, is elevated by some tall buildings that jut above others. The area-weighted average building height would then be unsuitable as a geometrical index of urban canopies with large height variations. Thus, the height of the upper envelope of the canopy was proposed as the representative canyon height.

1. Introduction

The zero-plane displacement height, *d*, is a key parameter that expresses the vertical profile of wind speed and other statistics over canopies through the Monin-Obukhov similarity theory (MOS). Although the concept of zero-plane displacement is not new, recent studies motivated us to consider *d* more precisely in complex terrains. Kurita and Kanda (2009) discussed the transition of wind speed profile across changes in land cover. They proposed different transition processes for the mean speed, which determines *d*, and the wind shear. The value of *d* in urban areas is one of the recent topics attracting attention not only out of pure meteorological interest but also from the viewpoint of its application. A precise estimation of *d* in an urban area is required for numerical studies that seek to clarify the urban impact on heavy rainfall (Matheson and Ashie 2008).

There are a number of methodologies to determine *d*. The following three approaches determine *d* by fitting measured variables into the MOS equation. A) Mean wind speed profile measurement (Mikami et al. 1996) is a conventional way in which multi-level wind speed is fitted to the logarithmic profile equation. B) Single-level turbulence measurements can also determine *d*. Rotach (1994) used temperature variance data; similarly, Toda and Sugita (2003) used vertical wind speed variance and Martano (2000) used mean wind speed. C) Multi-level heat flux measurement by scintillometers determines *d* (Kanda et al. 2002). All of these methodologies directly evaluate *d*. Other ways of indirect estimation utilize the fact that *d* is related to the canopy geometry. These approaches establish an empirical formula relating *d* to the canopy geometry or land use. D) The empirical relationship between *d* and land use could be useful in applying to satellite data (Rooney et al. 2005). E) Morphologic methods that relate *d* to geometrical parameters of buildings are often used to estimate *d* in urban areas. Such morphologic methods have the merit of being easy to use with Geographical Information Systems (GIS). However, they do not always agree well with direct measurements (Grimmond and Oke 1999).

This disagreement could partly be due to the variation of building height in a real city. Most morphologic methods are based on the results of experiments with roughness obstacles of homogeneous height. Zaki et al. (2011) conducted wind tunnel experiments and showed that height variation would make *d* larger than in the case of homogeneous roughness. Buildings in Tokyo are much more heterogeneous than those in Europe. The ratio of building height variance to the mean building height (σ_H/H_{av}) is 0.2 to 0.4 in European cities (Ratti et al. 2002), whereas it is 0.69 in the built-up district of Tokyo (Nakamura et al. 2000) and > 1.0 in the present study area. Therefore, experimental validation of the morphologic method is needed for Japanese cities. The present study measures *d* in the central built-up area of Tokyo according to the temperature variance method (Rotach 1994, hereafter TVM) and the scintillometer heat flux method (Kanda et al. 2002, hereafter SHM). Although the method using the wind speed profile (method A) appears to be the most reliable, it is impossible with the limited platforms for measurement in cities.

2. Site description and measurement

Measurements were taken in the Ginza area of downtown Tokyo (Fig. 1) in the summer of 2009. Although the terrain is almost flat, we can see the uneven heights of buildings and the sea water in the south. The study area is divided into four 45°-wide sectors in the analysis (Fig. 2). The vertex is the MRC, which houses the instruments (Fig. 1). Figure 3 shows a histogram of the building areas for each sector. As noted in the introduction, building height in the study area have larger variation than those of European cities, e.g., London. Table 1 summarizes urban canopy geometries in each sector. H_{av}, is an average of building height whose weight is ratio of roof area to lot area.

A sonic anemometer (Kaijo SAT-550) was installed at 110 m AGL in the roof-top radio tower (MRC). The sensor height was 60 m above the roof of MRC building. The anemometer was placed at the SE side of the tower to avoid distortions by the tower

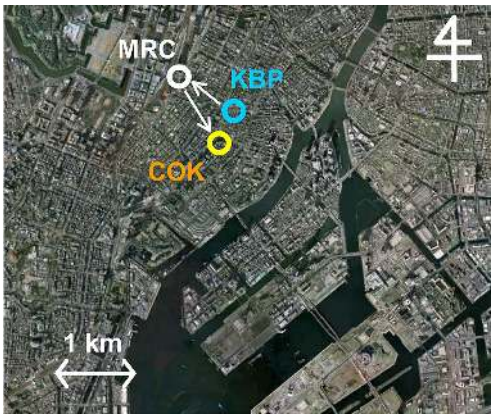

Fig. 1. Study area. MRC; sonic anemometer, upper receiver, and lower transmitter of scintillometer, COK; lower receiver, and KBP; upper transmitter of scintillometer.

Corresponding author: Hirofumi Sugawara, Earth and Ocean Sciences, National Defense Academy, 1-10-20 Hashirimizu, Yokosuka, Kanagawa, 239-8686, Japan. E-mail: hiros@nda.ac.jp.

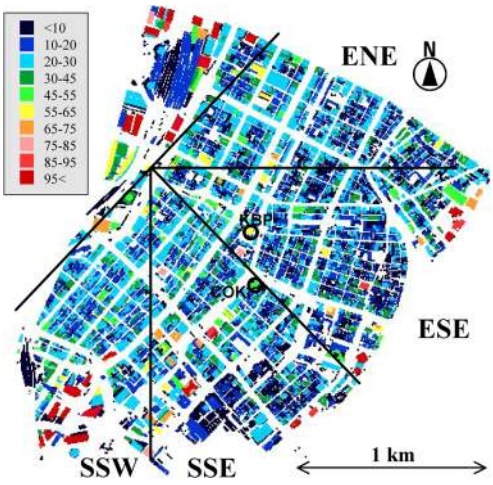

Fig. 2. Height of buildings (m) and definition of four sectors in the analysis. The vertex is the MRC tower. Building GIS data were provided by Tokyo Digital Map Corporation.

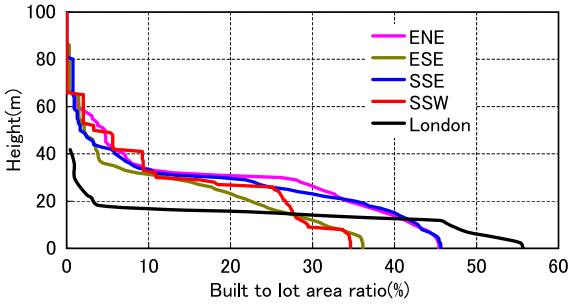

Fig. 3. Built-to-lot area ratio. Buildings are counted in different fetch lengths for each sector (shown in Section 3). The line for London is from Ratti et al. (2002).

Table 1. Canopy geometries. Calculated in different fetch lengths for each sector (shown in Section 3). H_{av}, area-weighted average of building height; σ_H, standard deviation of building heights; λ_p, plane area ratio of buildings to lot area.

	ENE	ESE	SSE	SSW
H_{av} (m)	13.6	9.4	12.9	10.5
σ_H/H_{av}	1.04	1.41	1.04	1.40
λ_p	0.45	0.36	0.46	0.35

Table 2. Setup of two scintillometers.

	Upper path		Lower path	
	trans.	rec.	trans.	rec.
location (Fig. 1)	KBP	MRC	MRC	COK
height (AGL m)	73	100	67	55
path length (m)	648		823	

in the dominant wind direction. An infrared gas analyzer (Li-COR LI-7500) and a radiometer (Kipp & Zonen CNR-1) were also installed in the tower at 110 m AGL. Air temperature, humidity, and static pressure were also measured with slow-response sensors. Turbulence data were recorded at a sampling rate of 10 Hz. Other data were recorded every minute.

Two sets of large-aperture scintillometers (Scintec BLS-900) measured the scintillation of light at different levels above the roof. Light pulse was emitted at 1 Hz. The light scintillation data were stored every minute and averaged across 30 min. Table 2 summarizes their configurations and Fig. 1 shows their optical paths.

Note that their heights were above the average building height but lower than those of some tall buildings shown in Fig. 3. The paths are likely to have been in the roughness sublayer. However, the few buildings taller than the scintillometer paths were at least 300 m away (Fig. 2). The distance/height ratio between the paths and those high-rise buildings was more than 3, thus the wake of those buildings would not be serious. In addition, Meijninger et al. (2002) showed that a scintillometer could be used below the blending height. Therefore, we can presume validity of scintillometer in our site. In this study, the scintillometer measurements were validated with the eddy covariance heat flux (described later).

3. Temperature variance method

The temperature variance method (TVM; Rotach 1994) uses the measured variance of temperature σ_T and its Monin-Obukhove similarity equation,

$$\frac{\sigma_T}{T_*} = -C_1\left(C_2 - \frac{z-d}{L}\right)^{-1/3} \quad (1)$$

to determine the unknown d with the least mean square method. Here T^* is the friction temperature, z is the sensor height, and L is the Obukhov length scale. The empirical constants C_1 and C_2 were 0.99 and 0.06, respectively, following Toda and Sugita (2003). Strictly speaking, the zero-plane displacement evaluated by the TVM may be different from that evaluated by wind speed or other scalars. However, the present study assumes that the value of d is the same for all meteorological variables. This is a common assumption in boundary-layer meteorology (Brutsaert 1982, page 60).

In the analysis, σ_T measured at MRC in each 30-min run was used. Vapor correction was applied to the sonic temperature and anemometer axis rotation (McMillen 1988). To check data quality, the temperature power spectrum was tested for a −2/3 slope and a peak at around $f = 0.1$ in each 30-min run. Data for sensible heat flux $Q_H < 200$ W m^{-2} or $z/L > -0.3$ were discarded because the sensor (110 m AGL) could exceed the atmospheric boundary layer. d was evaluated in each sector shown in Fig. 2. Data in northwest side of the tower would be contaminated by tower distortions.

Figure 4 shows the non-dimensional temperature variance as a function of $-z/L$ in sector SSW. Classification of sectors is based on the wind direction and the lateral extent of source area is not considered. The data are grouped by the fetch length from the MRC (the far end distance of source area, e, in Schmid 1994) along the wind direction. Note that the location of the source area is strongly related to the atmospheric stability. Table 3 shows d evaluated for different values of e. There are significant decreases in d for longer distances of e. Although these decreases could partly be due to the land-cover distribution, it should mainly be due to the influence of the flat surface of sea water spread over ~2 km south of the MRC. Avoiding sea-influenced suspicious data, we adopt d = 26 m in e = 200−400 m for sector SSW. A

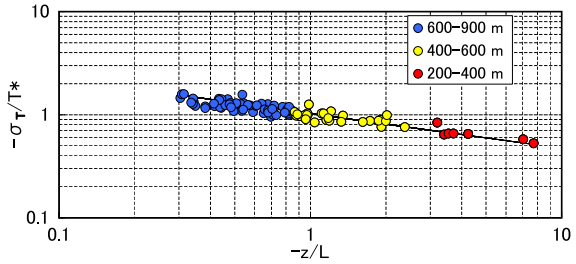

Fig. 4. Non-dimensional temperature variance as a function of atmospheric stability in sector SSW. Circles are measured data for each fetch length. The slope of the line is −1/3.

Table 3. Evaluated d for different values of fetch length *e*.

e (m)	200–400	200–600	200–900
d (m)	26	18	16

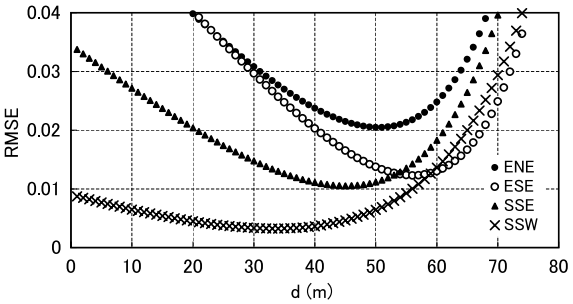

Fig. 5. RMSE of Eq. (1) in TVM.

similar analysis was applied to other sectors. In sector SSE, *d* was determined as 43 m, which corresponds to an e of 200−600 m. In sectors ENE and ESE, there was no significant dependence of *d* on fetch length, and d was determined for $e = 200$−900 m.

Figure 5 shows the RMSE in fitting Eq. (1) to the measured data. The minimum RMSE is on the order of 0.01 for every wind sector. Error analyses following Toda and Sugita (2003) revealed that the error in resulting *d* should be 15 m. The relatively gentle curve for SSW indicates that the evaluation of *d* is less robust against measurement error in this sector compared to other sectors.

4. Scintillometer heat flux method

The scintillometer is an optical instrument that measures light fluctuation and calculates the surface heat flux using MOS. Simultaneous measurement by two scintillometers at different heights can determine *d* assuming a constant flux between the two levels. This can be written as

$$Q_H(z_1 - d) = Q_H(z_2 - d) + Q_a. \tag{2}$$

Here, z_i is the measurement height at ith-level and $Q_H(z_i)$ is the heat flux at z_i. Q_a, which is the heat storage in the airmass between two levels, can be evaluated from a time series of measured air temperature. Kanda et al. (2002) introduced this scintillometer heat flux method (SHM) for a displaced-beams scintillometer and measured *d* in a suburban area of Tokyo. The present study attempted the SHM with a large aperture scintillometer (LAS). One of the significant characteristics of the scintillometer is the size of the flux source area, which is larger than that of the sonic anemometer. Therefore, the *d* obtained by the SHM should represent a larger area than that obtained by the TVM.

The LAS measures fluctuations in the refractive index, and thus the structure function coefficient for temperature, C_T^2, in the air between the transmitter and the receiver. We can obtain the heat flux Q_H by applying the measured C_T^2 to MOS.

$$\frac{(z-d)^{2/3} C_T^2}{T_*^2} = 4.9\left(1 + 6.1\left|\frac{z-d}{L}\right|^{-2/3}\right). \tag{3}$$

There are two options for measuring Q_H by the LAS (Lagouarde et al. 2006). The first is the mixed convection method, in which u^* is given by other methods such as turbulence measurements with a sonic anemometer. The second, known as the free convection method, must be applied to the unstable condition ($L \to -\infty$), where Eq. (3) leads to

$$Q_H = 1.05\frac{1}{\beta}k(z-d)\left(\frac{g}{T_a}\right)^{1/2}(C_T^2)^{3/4}. \tag{4}$$

Here, β is the Obukhov-Corrsin constant (0.86), k is the von Karman constant (0.4), g is the gravitational acceleration, and T_a is the mean air temperature. The mixed convection method requires that friction velocity u^* be given; it is inadequate for evaluating *d* because *d* can also be obtained from u^* (Grimmond and Oke 1999). The present study used the free convection method, where *d* was evaluated analytically by Eqs. (2) and (4) for each measurement run. To check the quality of scintillometer measurements in the roughness sublayer, the runs used in the analysis satisfied the condition that the Q_H values between the scintillometer and eddy covariance methods agree within 20 W m^{-2}.

Figure 6 shows the value of *d* in each run. Asanuma and Iemoto (2007) showed that the free convection method is applicable to $-z/L > 0.5$. In our data, *d* does not appear to depend on $-z/L$ in this range. We used runs for which $-z/L > 0.5$ in the analysis. This led to the result that the fetch length in each run was less than 900 m. In the TVM, a different fetch length was specified for each sector (Section 3); on the other hand, we used the same fetch length for all sectors in the SHM. This is because the scintillometer has a wider source area than the sonic anemometer, and because influence of flat sea water was seen in sectors SSE and SSW in Fig. 6.

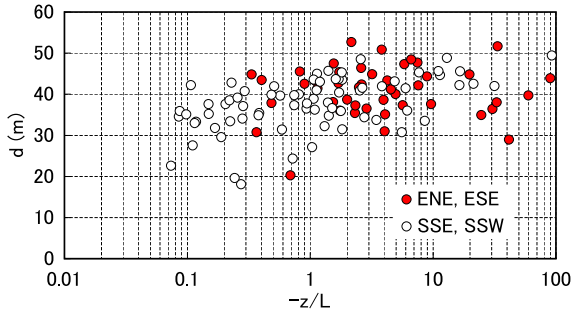

Fig. 6. *d* from SHM as a function of atmospheric stability. Note that fetch length is smaller at more unstable conditions.

5. Results and discussions

Although the source areas do not completely overlap between the TVM and SHM, their independent evaluations show reasonable agreement in Fig. 7. This means that either method performs well. SHM evaluations show less variation between sectors than TVM evaluations, presumably because of the larger source area in the scintillometer. Reductions in sectors SSE and SSW might still be influenced by the flat sea surface. As noted before, measurement errors make TVM evaluations less reliable, especially in sector SSW.

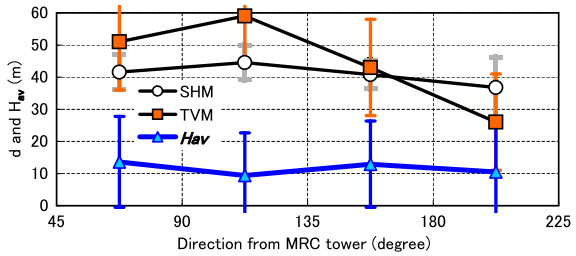

Fig. 7. Zero-plane displacement derived from TVM and SHM. Error bars for the TVM were evaluated from the RMSE. Those for the SHM and H_{av} indicate the standard deviation.

In every sector, values of d exceed the mean building height. Some tall buildings that jut above others surrounding them would make d larger even if their roof areas are small. d is the point of effect for wind drag (Jackson 1981), and a higher wind speed at a higher altitude has a greater effect on buildings. Zaki et al. (2011) also showed that d is larger than mean roughness height in canopies of heterogeneous height.

They showed that d increases as σ_H, increases. However, this could not be confirmed in Table 1 and Fig. 7. Changing our point of view, we will discuss the representative canopy height (H_{can}). In a heterogeneous building canopy with height variation, the area-weighted average building height would be problematic as the H_{can}. Some other weighting procedures such as those in Ratti et al. (2002) should be considered. Here, we attempt to determine H_{can} from the resultant d. The morphologic evaluation by Macdonald et al. (1998) determines normalized d, which in the present case is $(d/H_{can})_{MC}$. Assuming that $(d/H_{can})_{MC}$ is valid for a heterogeneous canopy, H_{can} is calculated with d obtained by the TVM as

$$H_{can} = \frac{d_{TVM}}{(d/H_{can})_{MC}}. \quad (5)$$

Note that the morphologic method by Macdonald et al. (1998) was established experimentally in a homogeneous canopy, and $(d/H_{can})_{\mathrm{MC}}$ can be calculated only from the plane area ratio. The assumption here can be reworded as follows: d/H_{can} in a heterogeneous canopy with height variation is the same as that in a homogeneous canopy if the scaling of H_{can} is successful in the heterogeneous canopy. Table 4 shows the H_{can} calculated by Eq. (5). Although the resultant H_{can} value differs by more than 10 m depending on which method (TVM or SHM) is used, it agrees with H_{max}, the maximum height in the sector. In sector SSE, the second highest building was 65 m, in agreement with H_{can}. That H_{can} and H_{max} agree indicates that the representative height of the canopy should be at the upper envelope of the canopy and not at the area-weighted average building height. H_{can} varies greatly depending on the methodology (TVM or SHM); therefore, the definition of the upper envelope may unfortunately be vague in this study. It should be somewhat lower than the highest building; for example, it might be the 90th percentile of building heights.

Table 4. Summary of H_{can} evaluation by Eq. (5).

	ENE	ESE	SSE	SSW
$(d/H_{can})_{\mathrm{MC}}$	0.72	0.63	0.73	0.61
H_{can} (TVM, m)	71	94	59	43
H_{can} (SHM, m)	58	71	56	61
H_{max} (m)	68	87	81	66

6. Conclusions

The zero-plane displacement height d in cities is often evaluated from building geometries. However, the performance of such morphologic methods is rather poor. Based on the hypothesis that unevenness of building heights causes this failure, this study measured d in the Ginza area of down town Tokyo, where the height variation of buildings is significant ($\sigma_{\mathrm{H}}/H_{av} > 1$). Two independent methods, the temperature variance and scintillometer heat flux methods, were used to evaluate d from measured data. Even when the measurement error is considered, the values of d obtained by either method exceed the average building height. The representative canopy height was estimated inversely from the measured d and the morphologic method. The height of the canopy envelope, rather than the area-weighted average of building height, was suggested as the canopy height.

Acknowledgments

The authors thank the Tokyo metropolitan government and Ministry of the Environment for the help in observations. This study is supported by the Obayashi Foundation and Grants-in-Aid for Scientific Research (C) 20560554.

References

Asanuma, J., and K. Iemoto, 2007: Measurements of regional sensible heat flux over Mongolian grassland using large aperture scintillometer. *J. Hydrology*, **333**, 58−67.

Brutsaert, W., 1982: Evaporation into the atmosphere: theory, history, and applications. Springer Netherlands, 316 pp.

Grimmond, C. S. B., and T. R. Oke, 1999: Aerodynamic properties of urban areas derived from analysis of surface form. *J. Appl. Meteor.*, **38**, 1262−1292.

Jackson, P. S., 1981: On the displacement height in the logarithmic velocity profile. *J. Fluid Mech.*, **111**, 15−25.

Kanda, M., R. Moriwaki, M. Roth, and T. Oke, 2002: Area-averaged sensible heat flux and a new method to determine zero-plane displacement length over an urban surface using scintillometry. *Bound.-Layer Meteor.*, **105**, 177−193.

Kurita, S., and M. Kanda, 2009: Characteristics of boundary layer over a sequence of small localized urban canopies with various heights obtained by wind-tunnel experiment. *J. Meteor. Soc. Japan*, **87**, 705−719.

Lagouarde, J.-P., M. Irvine, J.-M. Bonnefonde, C. S. B. Grimmond, N. Long, T. R. Oke, J. A. Salmond, and B. Offerle, 2006: Monitoring the sensible heat flux over urban areas using large aperture scintillometry: case study of Marseille city during the ESCOMPTE Experiment. *Bound.-Layer Meteor.*, **118**, 449−476.

Macdonald, R. W., R. F. Griffiths, and D. J. Hall, 1998: An improved method for the estimation of surface roughness of obstacle arrays. *Atmos. Environ.*, **32**, 1857−1964.

Martano, P., 2000: Estimation of surface roughness length and displacement height from single-level sonic anemometer data. *J. Appl. Meteor.*, **39**, 708−715.

Matheson, M. A., and Y. Ashie, 2008: The effect of changes of urban surfaces on rainfall phenomenon as determined by a non-hydrostatic mesoscale model. *J. Meteor. Soc. Japan*, **86**, 733−751.

McMillen, R. T., 1988: An eddy correlation technique with extended applicability to non-simple terrain. *Bound.-Layer Meteor.*, **43**, 231−245.

Meijninger, W. M. L., O. K. Hartogensis, W. Kohsiek, J. C. B. Hoedjes, R. M. Zuurbier, and H. A. R. De Bruin, 2002: Determination of area-averaged sensible heat fluxes with a large aperture scintillometer over a heterogeneous surface − Flevoland Field Experiment. *Bound.-Layer Meteor.*, **105**, 37−62.

Mikami, M., T. Toya, and N. Yasuda, 1996: An analytical method for the determination of the roughness parameters over complex regions. *Bound.-Layer Meteor.*, **79**, 23−33.

Nakamura, O., K. Miyashita, Y. Uematsu, and M. Yamada, 2000: Actual conditions of terrain roughness evaluated from numerical data of structural dimensions in Tokyo. *J. of Wind Engineering*, **84**, 59−69, (in Japanese with English abstract).

Ratti, C., S. Di Sabatino, R. Britter, M. Brown, F. Caton, and S. Burian, 2002: Analysis of 3-D urban databases with respect to pollution dispersion for a Number of European and American Cities. *Water, Air, & Soil Pollution: Focus*, **2**, 459−469.

Rooney, G. G., I. D. Longley, and J. F. Barlow, 2005: Variation of urban momentum roughness length with land use in the upwind source area, as observed in two U. K. cities. *Bound.-Layer Meteor.*, **115**, 69−84.

Rotach, M. W., 1994: Determination of the zero plane displa-cement in an urban environment. *Bound.-Layer Meteor.*, **67**, 187−193.

Schmid, H. P., 1994: Source areas for scalars and scalar fluxes. *Bound.-Layer Meteor.*, **67**, 293−318.

Toda, M., and M. Sugita, 2003: Single level turbulence measurements to determine roughness parameters of complex terrain. *J. Geophys. Res.*, **108**, ACL8.1−8.9.

Zaki, S. A., A. Hagishima, J. Tanimoto, and N. Ikegaya, 2011: Aerodynamic parameters of urban building arrays with random geometries. *Bound.-Layer Meteor.*, **138**, 99−120.

Manuscript received 14 April 2011, accepted 7 June 2011
SOLA: http://www.jstage.jst.go.jp/browse/sola